Accepted Manuscript

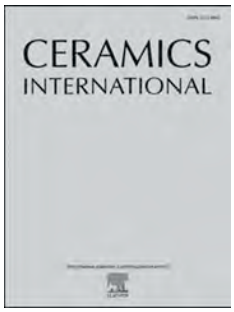

Structural, infrared reflectivity spectra and microwave dielectric properties of the $Li_7Ti_3O_9F$ ceramic

Zhiwei Zhang, Liang Fang, Huaicheng Xiang, Minyu Xu, Ying Tang, Heli Jantunen, Chunchun Li

PII: S0272-8842(19)30361-X

DOI: https://doi.org/10.1016/j.ceramint.2019.02.065

Reference: CERI 20788

To appear in: *Ceramics International*

Received Date: 23 January 2019

Revised Date: 10 February 2019

Accepted Date: 10 February 2019

Please cite this article as: Z. Zhang, L. Fang, H. Xiang, M. Xu, Y. Tang, H. Jantunen, C. Li, Structural, infrared reflectivity spectra and microwave dielectric properties of the $Li_7Ti_3O_9F$ ceramic, *Ceramics International* (2019), doi: https://doi.org/10.1016/j.ceramint.2019.02.065.

Structural, infrared reflectivity spectra and microwave dielectric properties of the $Li_7Ti_3O_9F$ ceramic

Zhiwei Zhang[1], Liang Fang[1, 3*], Huaicheng Xiang[1], Minyu Xu[1], Ying Tang[1], Heli Jantunen[4], Chunchun Li[1, 2*]

[1]*Guangxi universities key laboratory of non-ferrous metal oxide electronic functional materials and devices, College of Material Science and Engineering, Guilin University of Technology, Guilin, 541004, China*

[2]*College of Information Science and Engineering, Guilin University of Technology, Guilin, 541004, China*

[3]*College of Materials and Chemical Engineering, China Three Gorges University, Yichang, 443002, China*

[4]*Microelectronics Research Unit, Faculty of Information Technology and Electrical Engineering, University of Oulu, P. O. BOX 4500, FI-90014 Oulu University, Finland*

Abstract

A cubic rock salt structured ceramic, $Li_7Ti_3O_9F$, was fabricated via the conventional solid-state reaction route. The synthesis conditions, sintering characteristics, and microwave dielectric properties of $Li_7Ti_3O_9F$ ceramics were investigated by X-ray diffraction (XRD), thermal dilatometer, Scanning Electron Microscopy (SEM) accompanied with EDS mapping, and microwave resonant measurements. Rietveld refinement, selected area electron diffraction (SAED) pattern and high-resolution transmission electron microscopy (HRTEM) confirmed that $Li_7Ti_3O_9F$ adopts a cubic rock-salt structure. The ceramic sintered at 950 ^oC presented the optimal microwave properties of ε_r = 22.5, $Q\times f$ = 88,200 GHz, and τ_f = -24.2 ppm/^oC. Moreover, good chemical compatibility with Ag was verified through cofiring at 950 ^oC for 2 h. These results confirm a large potential for $Li_7Ti_3O_9F$ ceramic to be utilized as substrates in the low temperature cofired ceramic (LTCC)

* Corresponding Author, fanglianggl001@aliyun.com; lichunchun2003@126.com

technology. This work provides the possibility to exploit low-temperature-firing ceramics through solid solution between oxides and fluorides.

Keywords: Microwave dielectric ceramic; Low-temperature cofired ceramic technology (LTCC); Oxyfluoride; $Li_7Ti_3O_9F$

1. Introduction

Recent progress in the Internet of Things (IoT), microwave telecommunications, Tactile Internet (5th generation wireless systems), and satellite broadcasting has led to an increasing demand for low-loss dielectric materials [1, 2]. For practical applications, the critical properties required are an appropriate dielectric constant (ε_r), a high quality factor ($Q\times f$), a near-zero temperature coefficient of resonant frequency (τ_f), and a coefficient of thermal expansion (CTE) matched with other materials in integrations, etc. [3-5]. The toxicity and cost-effectiveness of the materials should also be considered [6]. Moreover, in order to meet the requirements of the low-temperature cofired ceramics (LTCC) technology, the ceramics should also be sintered below 960 ^{o}C to allow them to be cofired with a low-cost Ag electrode. Of primary significance is the low sintering temperature of LTCC technology which decreases energy consumption resulting in cost reductions, and less impact on the environment [7, 8].

Rock salt structured Li_2TiO_3 has recently been reported to possess good microwave dielectric properties (ε_r = 22.0, $Q\times f$ = 63,500 GHz, and τ_f = 20.3 ppm/^{o}C) [9]. However, the porous microstructure caused by lithium evaporation was reported to be a primary challenge for its practical applications. In addition, Li_2TiO_3 undergoes an order-disorder phase transition at 1215 ^{o}C, which makes it difficult to obtain a pure

Li_2TiO_3 phase with high densification [10-12]. Attempts have been made to improve the low densification of Li_2TiO_3 through non-stoichiometry modulation and solid solution modifications, such as $Li_{2+x}TiO_3$ [12], and $Li_{2x}Mg_{1-x}Ti_xO_{1+2x}$ [13]. Particularly, in the latter system, a number of low-loss rock salt structured dielectric materials have been designed in the Li_2TiO_3-MgO solid solution [15-20]. In spite of a the dramatically improved microstructure and enhanced quality factors with respect to the end-member Li_2TiO_3, the sintering temperatures were unfortunately raised which limits their actual applications in the LTCC technology.

LiF has a face-centered cubic rock salt structure, which is similar to that of Li_2TiO_3 being a superstructure with an edge-sharing cation oxygen octahedral structure [22-24]. Therefore, partial or complete solid solution between Li_2TiO_3 and LiF is expected. Moreover, LiF is commonly used as a sintering aid to improve the sintering behavior of ceramics due to its low melting point (848 ^oC) [25-26]. Herein, a glass-free low-temperature fired microwave dielectric ceramic $Li_7Ti_3O_9F$ was designed. Its crystal structure, microstructure, and microwave dielectric properties were studied in detail. The chemical compatibility of $Li_7Ti_3O_9F$ ceramics with Ag was also investigated.

2. Experimental procedure

$Li_7Ti_3O_9F$ samples were prepared via the solid-state reaction using high-purity Li_2CO_3 (99.99%，Guo-Yao Co. Ltd., Shanghai, China), TiO_2 (99.99%， Guo-Yao Co. Ltd., Shanghai, China), and LiF (99.99%，Xilong Chemicals, Guangdong, China) powders as starter materials. The raw powders were weighed according to the

stoichiometry and ball-milled with ZrO_2 balls and alcohol as milling media in a polyethylene jar for 6 h. After drying at 120 ^oC, the mixtures were calcined at 800 ^oC for 2 h, and then re-milled for 6 h. The compound was dried and granulated with 5 wt % PVA as binder, and then pressed into cylinders under a pressure of 150 MPa. The cylinders were heated at 550 ^oC for 2 h to burn out the PVA and then subsequently sintered at 875–975 ^oC for 2 h. In order to minimize the volatilization of lithium during sintering, the samples were covered with sacrificial powders with the same composition. To investigate the chemical compatibility of $Li_7Ti_3O_9F$ with Ag electrodes, the compounds were mixed with 20 wt% silver powders and cofired at 950 ^oC for 2 h.

The phase formation of $Li_7Ti_3O_9F$ was studied by XRD (Panalytical X'pert Pro diffractometer with Cu Kα radiation). Rietveld refinement was performed on the XRD data using Topas-Academic software. The bulk densities of samples were determined using the Archimedes method. The microstructure and energy-dispersive X-ray spectroscopy (EDS) analyses were performed using a Hitachi S4800 scanning electron microscope (SEM). Room-temperature Raman spectra were recorded using a Thermo Fisher Scientific DXR Raman spectrometer. The high-resolution transmission electron microscope (HRTEM) images and the selected-area electron diffraction (SAED) patterns were collected by a JEOL JEM-2100F TEM. XPS measurements were performed with an ESCALAB 250Xi X-ray photoelectron spectrometer with monochromatized Al Kα radiation. Microwave dielectric properties were measured by an Agilent N5230A network analyzer and a Delta 9039 oven. The τ_f value was

measured in the temperature range of 25-85 ^{o}C. The linear coefficient of thermal expansion (α_L) of the ceramics was measured by a NETZSCH DIL402C thermal dilatometer.

3. Results and discussion

XRD patterns of the $Li_7Ti_3O_9F$ ceramics fired at various temperatures are shown in Fig. 1 (a). A cubic rock-salt structure was identified based on PDF# 03-1024 of Li_2TiO_3 (α-Li_2TiO_3 (SS), Fm-3m) and no secondary phase was detected. Fig. 1 (b) shows the Rietveld refinement plots of $Li_7Ti_3O_9F$ ceramics sintered at 950 ^{o}C. The cell parameters were refined as $a = b = c = 4.1340(1)$ Å, and $V_m = 70.6541(8)$ Å^3. The schematic crystal structure is shown in the inset of Fig. 1 (b), which can be described as O/F anions randomly stacking in a cubic close packing with Li/Ti cations occupying the octahedron sites. To further confirm the structure of the $Li_7Ti_3O_9F$ sample, a selected area electron diffraction (SAED) pattern and high-resolution transmission electron microscopy (HRTEM) were performed. Fig. 1 (c) and (d) present the SAED patterns and HRTEM images of $Li_7Ti_3O_9F$ ceramic recorded along the [001] zone axis. The SAED pattern and the lattice fringes of the sample display interplanar spacing in the particle and were well matched with the cubic rack model (space group:Fm-3m, No.225). In conclusion, these results indicated that $Li_7Ti_3O_9F$ is a cubic structure, which is consistent with the XRD refinement results.

Fig. 2 shows the naturally fresh surface morphologies of $Li_7Ti_3O_9F$ ceramics sintered at various temperatures and the element mapping of the constituents on the 950 ^{o}C sintered sample. The grain size distributions and the average grain size of

$Li_7Ti_3O_9F$ are given in the inset of Fig. 2 (a)-(e). At 900 ^oC, the grain size was relatively small between 6 ~ 12 μm, whereas the sample sintered at 950 ^oC had larger grains, about 14 ~ 20 μm. The average grain size increased from 7.78 μm to 19.98 μm when the temperature increased from 875 ^oC to 975 ^oC. A dense and homogeneous microstructure with an average grain size of ~ 16 μm was obtained in the sample sintered at 950 ^oC/2 h, (Fig. 2 (d)). However, partial melting together with abnormally large grains (~ 30 μm) and a small amount of porosity was clearly distinguished in the $Li_7Ti_3O_9F$ ceramic sintered at 975 ^oC. To analyze the element distributions, element mapping of the constituents on the 950 ^oC sintered sample is displayed in Fig. 2 (g)-(i). It is obvious that all elements (F, O, and Ti) were distributed homogeneously, and no element precipitation was observed at the grain boundary, further suggesting that LiF entered into the crystal lattice of Li_2TiO_3.

Fig. 3 shows the variations in bulk density and microwave dielectric properties of $Li_7Ti_3O_9F$ ceramic with sintering temperature in the range 875 to 975 ^oC. As the sintering temperature increased, the bulk density gradually increased to a maximum value of ~ 3.15 g/cm^3 with a relative density of 94.3% at 950 ^oC. It is well-known that many factors affect dielectric properties, such as lattice vibration, the density, ionic polarizability, order-disorder, grain boundaries, and secondary phase, etc. [27-32]. In this work, the dielectric constant steadily increased on increasing the sintering temperature from 875 to 950 ^oC, as a result of the increasing density. Similarly, the quality factor increased with increasing sintering temperature, reaching a maximum value of 88,200 GHz at 950 ^oC. In contrast, the temperature coefficient of resonant

frequency of $Li_7Ti_3O_9F$ ceramics remained temperature independent, fluctuating at around -24 ppm/^oC (Fig. 3 (d)). The τ_f value is related to the temperature coefficient of the relative permittivity (τ_ε), and the linear thermal expansion coefficient, α_L, as follows [33]:

$$\tau_f = -\left(\frac{\tau_\varepsilon}{2} + \alpha_L\right) \quad (1)$$

From the CTE curve of $Li_7Ti_3O_9F$ ceramic sintered at 950 ^oC shown in Fig. 4 (a), the average linear thermal expansion coefficient α_L was calculated to be 11.20 ppm/^oC.

Fig. 4 (b) shows the temperature dependence of dielectric constant (ε_r) and loss tangent (*tan* δ) at various frequencies. ε_r and *tan* δ showed good temperature stability between room temperature and 180 ^oC. The profile measured at 1 MHz from 25 to 85 ^oC is shown in the inset of Fig. 4 (b), yielding a τ_ε value of 34.4 ppm/^oC, resulting in a τ_f value of -28.4 ppm/^oC according to Eq.1. This calculated value is a little higher than the value measured at microwave frequency (-24.2 ppm/^oC), which might be due to the different measurement frequency. Besides, it is worth mentioning that a frequency dispersion related to the thermally activated polarizability mechanisms was observed as the measurement temperature exceeded to 200 ^oC. The frequency dispersion responded instantly at low frequency but it lagged at high frequency [34]. As a result, a higher relative permittivity (ε_r ~ 39) at 1 MHz was measured compared to that at microwave frequency (ε_r ~ 22.5).

To study this high-frequency dielectric anomaly, X-ray photoelectron spectroscopy (XPS) was conducted on the $Li_7Ti_3O_9F$ sample sintered at 950 ^oC (Fig. 5 (a, b)). To clarify, the C element detected was introduced during the measurement

process. The Ti-2p regions in the sample were fitted well into the Gaussian sub peaks. Three dominant peaks (457.8 eV, 458.3 eV, and 464 eV) were clearly distinguished. According to the previous work, the 458.3 eV and 464 eV correspond to Ti^{4+} while the 457.8 eV is related to the Ti^{3+}2p peak [35, 36]. The ratio of $(Ti^{3+})/(Ti)_{total}$ was estimated to be approximately 2% based on the method proposed by Borchert *et al* [37]. It is well known that valence variation in titanium is ubiquitous, especially in oxides being sintered at elevated temperatures, and it is believed to be related to the released electrons due to the emergence of an oxygen vacancy [38-40]. The chemical defect equation can be expressed as follows:

$$O_O^x \Leftrightarrow V_O^x + \frac{1}{2}O_2 \quad (2)$$

$$V_O \Leftrightarrow V_O^{\cdot} + e' \quad (3)$$

$$V_O^{\cdot} \Leftrightarrow V_O^{\cdot\cdot} + e' \quad (4)$$

$$Ti_{Ti}^x + e' \Leftrightarrow Ti_{Ti}' \quad (5)$$

The negatively charged Ti_{Ti}' can bond weakly to the neighboring positively charged $V_O^{\cdot\cdot}$, resulting in defect dipoles, perhaps in the form of Ti_{Ti}'-$V_O^{\cdot\cdot}$-Ti_{Ti}'. These kinds of dipoles could offer a contribution to the dielectric properties, especially at low frequencies, but cannot follow the high-frequency change because of the large time constant, consequently giving rise to the manifest frequency dependence of the dielectric behaviors. Additionally, because of the weak-coupling energy, the bonding can be broken at a certain temperature, and thus, the unbonded point defects can move freely to some extent, yielding conductivity losses that contributes to the high-temperature rise in dielectric losses.

Fig. 6 shows the Raman spectra of $Li_7Ti_3O_9F$ ceramics sintered at 875-975 ^oC. A profile of a pure Li_2TiO_3 sample sintered at 1300 ^oC is also shown for comparison. After fitting by the Gaussian-Lorentzian function, seven Raman active modes at 140 cm^{-1}, 286 cm^{-1}, 348 cm^{-1}, 430 cm^{-1}, 710 cm^{-1}, 804 cm^{-1}, and 834 cm^{-1} were detected. Irrespective of their sintering temperatures, all the $Li_7Ti_3O_9F$ compositions showed similar profiles indicating structural stability over the temperature range studied. By comparison, the completely different Raman spectra for $Li_7Ti_3O_9F$ and Li_2TiO_3 indicate their different structure, which further reveals the solid solution between LiF and Li_2TiO_3.

The far infrared reflectivity spectrum is generally used to characterize the eigen dielectric properties of microwave ceramics [41] The measured and fitted IR reflectivity spectra of the $Li_7Ti_3O_9F$ ceramic in the range 50~1000 cm^{-1} are plotted in Figure 7(a). It can be seen that the infrared spectra can be well fitted by 6 resonant modes, and the related phonon parameters are listed in Table 1. These spectra were analyzed by using the classical harmonic oscillator model based on the standard Lorentzian formula [Eq (6)] and the Fresnel formula [Eq (7)]:[42, 43]

$$\varepsilon^*(\omega) = \varepsilon_\infty + \sum_{j=1}^{n} \frac{\omega_{pj}^2}{\omega_{oj}^2 - \omega^2 - j\omega\gamma_j} \quad (6)$$

$$R(\omega) = \left| \frac{1-\sqrt{\varepsilon^*(\omega)}}{1+\sqrt{\varepsilon^*(\omega)}} \right|^2 \quad (7)$$

where $\varepsilon^*(\omega)$ is a complex dielectric function, ε_∞ is the dielectric constant caused by the electronic polarization at high frequencies, γ_j, ω_{oj} and ω_{pj} are the damping factor, the transverse frequency and plasma frequency of the *j*-th Lorentz oscillator, respectively, and *n* is the number of transverse phonon modes; R(ω) is the IR

reflectivity. Figure 7(b) presents the measured and fitted real and imaginary parts of the permittivity. It was observed that the fitted value of ε_r was a little smaller than the measured values in the microwave range. Meanwhile, all the fitted dielectric permittivity and dielectric loss values were nearly equal to the measured ones using the $TE_{01\delta}$ method. Therefore, it can be concluded that the polarization of the $Li_7Ti_3O_9F$ ceramic in the microwave region was mainly attributed to the absorptions of phonon oscillation in the infrared region.

To investigate the chemical compatibility with the silver electrode, the $Li_7Ti_3O_9F$ ceramic powder was chosen to be cofired with 20 wt% silver (Ag) powders at 950 ^oC for 2 h. XRD patterns, a backscattered electron image (BSEM), and EDS analysis of the cofired samples are shown in Fig. 8. $Li_7Ti_3O_9F$ and Ag (PDF: 01-1164) phases were detected, indicating no chemical reaction between them. Additionally, the BSE image, as shown in the inset in Fig.8, shows two kinds of grains with different sizes and shapes, in which the larger ones may be identified as Ag with the help of elemental analysis by energy-dispersive X-ray spectroscopy (EDS). These features, in combined with the XRD analysis, confirm no chemical reaction between $Li_7Ti_3O_9F$ and silver.

Table 2 compares the reported sintering temperature and microwave dielectric properties of some rock salts being reported. The relative permittivity of $Li_7Ti_3O_9F$ is comparable to Li_2TiO_3 but higher than the other counterparts. The quality factor is superior to that of Li_2TiO_3 but inferior to the Mg-containing compounds. Most importantly, the sintering temperature of $Li_7Ti_3O_9F$ is extremely low, which is

comparable to that of Li_4WO_5. Most of the reported rock salt compounds need high possessing temperatures to densify. Until now, $Li_7Ti_3O_9F$ and Li_4WO_5 are the exceptional rock salts with a combination of low sintering temperature and outstanding microwave dielectric performances. These findings of merits support their potential utilization in LTCC technology.

4. Conclusions

A novel oxyfluoride, $Li_7Ti_3O_9F$, is designed and synthesized through solid solution between Li_2TiO_3 and LiF. XRD and Rietveld refinement confirm a cubic structure (Fm-3m) with a = 4.1340(1) Å. Sintering behavior optimization reveals that $Li_7Ti_3O_9F$ could be densified at relatively low sintering temperatures ≤ 950 ^oC with a dense microstructure, which is superior to that of the end-number Li_2TiO_3. Excellent microwave dielectric properties with ε_r = 22.5, $Q \times f$ = 88,200 GHz (with f = 9.2 GHz), and τ_f = -24.2 ppm/^oC were accessible in the sample being sintered at 950 ^oC. Additionally, $Li_7Ti_3O_9F$ has an average CTE of 11.2 ppm/^oC and good chemical compatibility with silver electrodes. The combined excellent dielectric performances, low thermal expansion, and good chemical compatibility make $Li_7Ti_3O_9F$ a promising alternative for LTCC applications. The present work may shed light on the design of low-temperature-firing materials through solid solution between oxides and fluorides.

Acknowledgments

We appreciate Dr. Jibran Khaliq from Northumbria University at Newcastle, UK, for his help in language polishing. This work was supported by the Natural Science Foundation of China (Nos. 21561008, 51502047 and 21761008), the Natural Science

Foundation of Guangxi Zhuang Autonomous Region (Nos. 2015GXNSFFA139003, 2016GXNSFBA380134, 2016GXNSFAA380018, and 2018GXNSFAA138175), and Project of Scientific Research and Technical Exploitation Program of Guilin(20170225).

References

[1] M. T. Sebastian, R. Ubic, H. Jantunen, Low-loss dielectric ceramic materials and their properties, Int. Mater. Rev. 60 (2015) 392-412.

[2] H. Ohsato, Functional advances of microwave dielectric for next generation, Ceram. Int. 38 (2012) S141-S146.

[3] N. Joseph, J. Varghese, T. Siponkoski, M. Teirikangas, M. T. Sebastian, H. Jantunen, Glass-free CuMoO4 ceramic with excellent dielectric and thermal properties for ultralow temperature cofired ceramic applications, ACS Sustainable Chem. Eng. 4 (2016) 5632-5639.

[4] R. J. Cava, Dielectric materials for applications in microwave communications, J. Mater. Chem. 11 (2001) 54-62.

[5] J. Varghese, T. Siponkoski, M. Teirikangas, M. T. Sebastian, A. Uusimaki, H. Jantunen, Structural, dielectric, and thermal properties of Pb free molybdate based ultralow temperature glass, ACS Sustainable Chem. Eng. 4 (2016) 3897-3904.

[6] M. T. Sebastian, H. Wang, H. Jantunen, Low temperature co-fired ceramics with ultra-low sintering temperature: A review, Curr. Opin. Solid State Mater. Sci. 20 (2016) 151-170.

[7] https://doi.org/10.1016/j.ceramint.2019.01.126

[8] C. C. Xia, D. H. Jiang, G. H. Chen, Microwave dielectric ceramic of LiZnPO4 for LTCC applications, J. Mater. Sci: Mater. Electron. 28 (2017) 12026–12031.

[9] L. L. Yuan, J. J. Bian, Microwave dielectric properties of lithium contained ceramics with rock salt structure, Ferroelectrics. 387 (2009) 123-129.

[10] P. Gierszewski, Review of properties of lithium metatitanate, Fusion Eng. Des. 39-40 (1998) 739-743.

[11] H. Kleykamp, Phase equilibria in the Li-Ti-O system and physical properties of Li_2TiO_3, Fusion Eng. Des. 61-62 (2002) 361-366.

[12] J. J. Bian, Y. F. Dong, Sintering behavior, microstructure and microwave dielectric properties of $Li_{2+x}TiO_3$ ($0 \leq x \leq 0.2$), Mater. Sci. Eng. B. 176 (2011) 147-151.

[13] H. F. Zhou, X. H. Tan, J. Huang, N. Wang, G. C. Fan, X. L. Chen, Phase structure, sintering behavior and adjustable microwave dielectric properties of $Mg_{1-x}Li_{2x}Ti_xO_{1+2x}$ solid solution ceramics, J. Alloys Compd. 696 (2017) 1255-1259.

[14] H. T. Wu, E. S. Kim, Characterization of low loss microwave dielectric materials $Li_3Mg_2NbO_6$ based on the chemical bond theory. J. Alloys Compd. 669 (2016) 134-140.

[15] Y. W. Tseng, J. Y. Chen, Y. C. Kuo, C. L. Huang, Low-loss microwave dielectrics using rock salt oxide Li_2MgTiO_4, J. Alloys Compd. 509 (2011) L308-L310.

[16] C. C. Li, H. C. Xiang, C. Z. Yin, Y. Tang, Y. C. Li, L. Fang, Ultra-Low Loss Microwave Dielectric Ceramic $Li_2Mg_2TiO_5$ and Low-Temperature Firing Via B_2O_3 Addition, Journal of ELECTRONIC MATERIALS. 47 (2018) 6383-6389.

[17] Z. F. Fu, P. Liu, J. L. Ma, X. G. Zhao, H. W. Zhang, Novel series of ultra-low loss microwave dielectric ceramics: $Li_2Mg_3BO_6$ (B = Ti, Sn, Zr), J. Eur. Ceram. Soc. 36 (2016) 625-629.

[18] J. X. Bi, C. C. Li, Y. H. Zhang, C. F. Xing, C. H. Yang, H. T. Wu, Crystal structure, infrared spectra and microwave dielectric properties of ultra low-loss $Li_2Mg_4TiO_7$ ceramics, Mater. Lett. 196 (2017) 128-131.

[19] J. X. Bi, Y. J. Niu, H. T. Wu, $Li_4Mg_3Ti_2O_9$: A novel low-loss microwave dielectric ceramic for LTCC, Ceram. Int. 43 (2017) 7522-7530.

[20] H. L. Pan, H. T. Wu, Crystal structure, infrared spectra and microwave dielectric properties of new ultra low-loss $Li_6Mg_7Ti_3O_{16}$ ceramics, Ceram. Int. 43 (2017) 14484-14487.

[21] J. Li, L. Fang, H. Luo, J. Khaliq, Y. Tang, C. C. Li, Li_4WO_5: A temperature stable low-firing microwave dielectric ceramic with rock salt structure, J. Eur. Ceram. Soc. 36 (2016) 243-246.

[22] N.V. Tarakina, R. B. Neder, T. A. Denisova, L. G. Maksinova, Y. V. Baklanova, A. P. Tyutyunnik, V. G. Zubkov, Defect crystal structure of new $TiO(OH)_2$ hydroxide and related lithium salt Li_2TiO_3, Dalton Trans. 39 (2010) 8168-8176.

[23] T. Fehr, E. Schmidbauer, Electrical conductivity of Li_2TiO_3 ceramics, Solid State Ionics. 178 (2007) 35-41.

[24] J. J. Bian, J. Y. Wu, L. Wang, Structural evolution, sintering behavior and microwave dielectric properties of $(1-x)Li_3NbO_4$-$xLiF$ ($0 \leq x \leq 0.9$), J. Eur. Ceram. Soc. 32 (2012) 1251-1259.

[25] U. Intatha, S. Eitssayeam, K. Pengpat, K.J.D. MacKenzie, T. Tunkasiri, Dielectric properties of low temperature sintered LiF doped $BaFe_{0.5}Nb_{0.5}O_3$, Matter. Lett. 61 (2007) 196-200.

[26] J. X. Tong, Q. L. Zhang, H. Yang, J. L. Zou, Low-temperature firing and microwave dielectric properties of $Ca[(Li_{0.33}Nb_{0.67})_{0.9}Ti_{0.1}]O_{3-\sigma}$ ceramics with LiF addition, Matter. Lett. 59 (2005) 3252-3255.

[27] Y. Tang, L. Fang, H. F. Zhou, Q. W. Liu, H. Zhang, Microwave dielectric properties and chemical compatibility with silver electrode of low-fired $Li_2Cu_{0.2}Mg_{0.8}Ti_3O_8$ ceramics, Ceram. Int. 39 (2013) 8503-8506.

[28] C. C. Li, H. C. Xiang, M. Y. Xu, Y. Tang, L. Fang, Li_2AGeO_4 (A = Zn, Mg):Two novel low-permittivity microwave dielectric ceramics with olivine structure, J. Eur. Ceram. Soc. 38 (2018) 1524-1528.

[29] D. Zhou, L. X. Pang, J. Guo, G. Q. Zhang, Y. Wu,; Wang, H.; Yao, X. Low temperature firing microwave dielectric ceramics $(K_{0.5}Ln_{0.5})MoO_4$ (Ln = Nd and Sm) with low dielectric loss. J. Eur. Ceram. Soc. 2011, 31, 2749-2752.

[30] Li, C. C.; Yin, C. Z.; Chen, J. Q. H. C. Xiang, Y. Tang, L. Fang, Crystal structure and dielectric properties of germanate melilites $Ba_2MGe_2O_7$ (M = Mg and Zn) with low permittivity, J. Eur. Ceram. Soc. 38 (2018) 5246-5251.

[31] S. George, M. T. Sebastian, Synthesis and microwave dielectric properties of novel temperature stable high Q, $Li_2ATi_3O_8$ (A = Mg, Zn) ceramics, J. Am. Ceram. Soc. 93 (2010) 2164-2166.

[32] C. C. Li, H. C. Xiang, M. Y. Xu, J. Khaliq, J. Q. Chen, L. Fang, Low-firing and temperature stable microwave dielectric ceramics $Ba_2LnV_3O_{11}$ (Ln = Nd, Sm), J. Am. Ceram. Soc. 101 (2018) 773-781.

[33] C. C. Chiang, S. F. Wang, Y. R. Wang, W. C. J. Wei, Densification and

microwave dielectric properties of CaO-B_2O_3-SiO_2 system glass-ceramics, Ceram. Int. 34 (2008) 599-604.

[34] H. C. Xiang, C. C. Li, H. Jantunen, L. Fang, A. E. Hill, Ultralow Loss CaMgGeO4 Microwave Dielectric Ceramic and Its Chemical Compatibility with Silver Electrodes for Low-Temperature Cofired Ceramic Applications, ACS Sustainable Chem. Eng. 6 (2018) 6458-6466.

[35] Z. Xiong, B. Tang, Z. X. Fang, C. T. Yang, S. R. Zhang, Effects of $(Cr_{0.5}Ta_{0.5})^{4+}$ on structure and microwave dielectric properties of $Ca_{0.61}Nd_{0.26}TiO_3$ ceramics, Ceram. Int. 44 (2018) 7771-7779.

[36] J. Khaliq, C. C. Li, K. Chen, B. G. Shi, H. T. Ye, A. M. Grande, H. X. Yan, M. J. Reece, Reduced thermal conductivity by nanoscale intergrowths in perovskite like layered structure $La_2Ti_2O_7$, J. Appl. Phys. 117 (2015) 075101-075107.

[37] H. Borchert, Y. V. Frolova, V. V. Kaichev, I. P. Prosvirin, G. M. Alikina, Electronic and chemical properties of nanostructured cerium dioxide doped with praseodymium, J. Phys. Chem. B. 109 (2005) 5728-5738.

[38] Z. X. Fang, B. Tang, F. Si, S. R. Zhang, Low temperature sintering of high permittivity Ca-Li-Nd-Ti microwave dielectric ceramics with $BaCu(B_2O_5)$ additives, J. Alloys. Compd. 693 (2017) 843-852.

[39] H. T. Chen, B. Tang, P. Fan, S. X. Duan, M. Wei, Y. Yuan, S. R. Zhang, Microwave dielectric properties of aluminum substituted $Ca_{0.6}Nd_{0.26}TiO_3$ ceramics, J. Ceram. Soc. Jpn. 124 (2016) 903-906.

[40] C. C. Li, X. Y. Wei, L. Fang, H. X. Yan, M. J. Reece, Dielectric relaxation and

electrical conductivity in $Ca_5Nb_4TiO_{17}$ ceramics, Ceram. Int. 41 (2015) 9923-9930.

[41] I. N. Lin, C. T. Chia, H. L. Liu, Intrinsic dielectric and spectroscopic behavior of perovskite Ba $(Ni_{1/3}Nb_{2/3})O_3$–$Ba(Zn_{1/3}Nb_{2/3})O_3$ microwave dielectric ceramics, J. Appl. Phys. 102 (2007) 044112.

[42] Z. Chen, H. Jia, K. Sharafudeen, W. B. Dai, Y. B. Liu, G. Q. Dong, J. R. Qiu, Up-conversion luminescence from single vanadate through blackbody radiation harvesting broadband near-infrared photons for photovoltaic cells, J. Alloy. Compd. 663 (2016) 204–210.

[43] J. Guo, D. Zhou, L. Wang, H. Wang, T. Shao, Z. M. Qi, X. Yao, Infrared spectra, Raman spectra, microwave dielectric properties and simulation for effective permittivity of temperature stable ceramics AMoO4–TiO2 (A = Ca, Sr). Dalton Trans. 42 (2013) 1483–1491.

Table 1 Phonon parameters obtained from the fitting of the infrared reflectivity spectra of $Li_7Ti_3O_9F$ ceramic.

Mode	ω_{oj}	ω_{pj}	γ_j	$\Delta\varepsilon_j$
1	133.88	318.76	134.99	5.6700
2	256.63	289.24	65.67	2.3300
3	306.42	1168	230.99	14.500
4	466.17	206.47	58.214	0.1960
5	673.36	378.91	179.19	0.3170
6	802.21	173.03	55.527	0.0465
	$Li_7Ti_3O_9F$	ε_∞=1.94	ε_0=23.06	

Table 2 The sintering temperature (S.T.) and microwave dielectric properties of some rock salts.

Ceramics	S.T. (^{o}C)	ε_r	$Q\times f$ (GHz)	τ_f (ppm/^{o}C)	Reference
Li_2TiO_3	1300	22	63,500	20.3	[9]
Li_2ZrO_3	1450	15.54	37,166	-26.6	[9]
Li_3NbO_4	1150	16.4	47179	-45	[9]
$Li_3Mg_2NbO_6$	1225	14.94	100,965	-21.96	[14]
Li_2MgTiO_4	1360	17.25	97,300	-27.2	[15]
$Li_2Mg_2TiO_5$	1320	13.4	95,000	-32.5	[16]
$Li_2Mg_3TiO_6$	1280	15.2	152,000	-39	[17]
$Li_2Mg_4TiO_7$	1600	13.43	233,600	-7.24	[18]
$Li_4Mg_3Ti_2O_9$	1450	15.97	135,800	-7.06	[19]
$Li_6Mg_7Ti_3O_{16}$	1550	15.27	209,400	-11.32	[20]
Li_4WO_5	890	8.6	23,100	-2.6	[21]
$Li_7Ti_3O_9F$	950	22.5	88,200	-24.2	this work

Figure Captions:

Fig. 1 (a) XRD patterns of $Li_7Ti_3O_9F$ ceramic sintered at 875-975 ^oC for 2 h. (b) Rietveld refinement of sample sintered at 950 ^oC and schematic of the crystal structure for $Li_7Ti_3O_9F$. (c) selected area electron diffraction (SAED) pattern of $Li_7Ti_3O_9F$ sample sintered at 950 ^oC. (d) high-resolution transmission electron microscopy (HRTEM) images of $Li_7Ti_3O_9F$ ceramic recorded along the [001] zone axis.

Fig. 2 FE-SEM images of the surfaces of the sintered ceramic at: (a) 875 ^oC, (b) 900 ^oC, (c) 925 ^oC, (d) 950 ^oC, (e) 975 ^oC for $Li_7Ti_3O_9F$ and corresponding EDS analysis surface scanning of (f) EDS spectrum (g) F element, (h) O element, (i) Ti element.

Fig. 3 The bulk density and microwave dielectric properties (ε_r, $Q\times f$, and τ_f) of $Li_7Ti_3O_9F$ ceramic sintered at different temperatures.

Fig. 4 (a) Thermal expansion curve in the temperature range 25-800 ^oC of $Li_7Ti_3O_9F$ sintered at 950 ^oC. (b) Dependence of relative permittivity (ε_r) on temperature and loss tangent (tanδ) at four different frequencies (1, 10, and 100 kHz and 1 MHz).

Fig. 5 (a) XPS survey scan of $Li_7Ti_3O_9F$ sample sintered at 950 ^oC for 2 h. (b) High-resolution XPS spectra for Ti-2p photoelectron peaks.

Fig. 6 Raman spectra of pure Li_2TiO_3 sample sintered at 1300 ^oC and $Li_7Ti_3O_9F$ ceramic sintered at 875-975 ^oC in the range of 80-1000 cm^{-1}.

Fig. 7 (a) The measured and fitted IR reflectivity spectra of the $Li_7Ti_3O_9F$ ceramic in

the range 50~1000 cm^{-1}. (b) The measured and fitted real and imaginary parts of permittivity.

Fig. 8 XRD and BSEM analysis of the cofired $Li_7Ti_3O_9F$ ceramic cofired with 20 wt% Ag at 950 ^oC for 2 h.

Fig.1

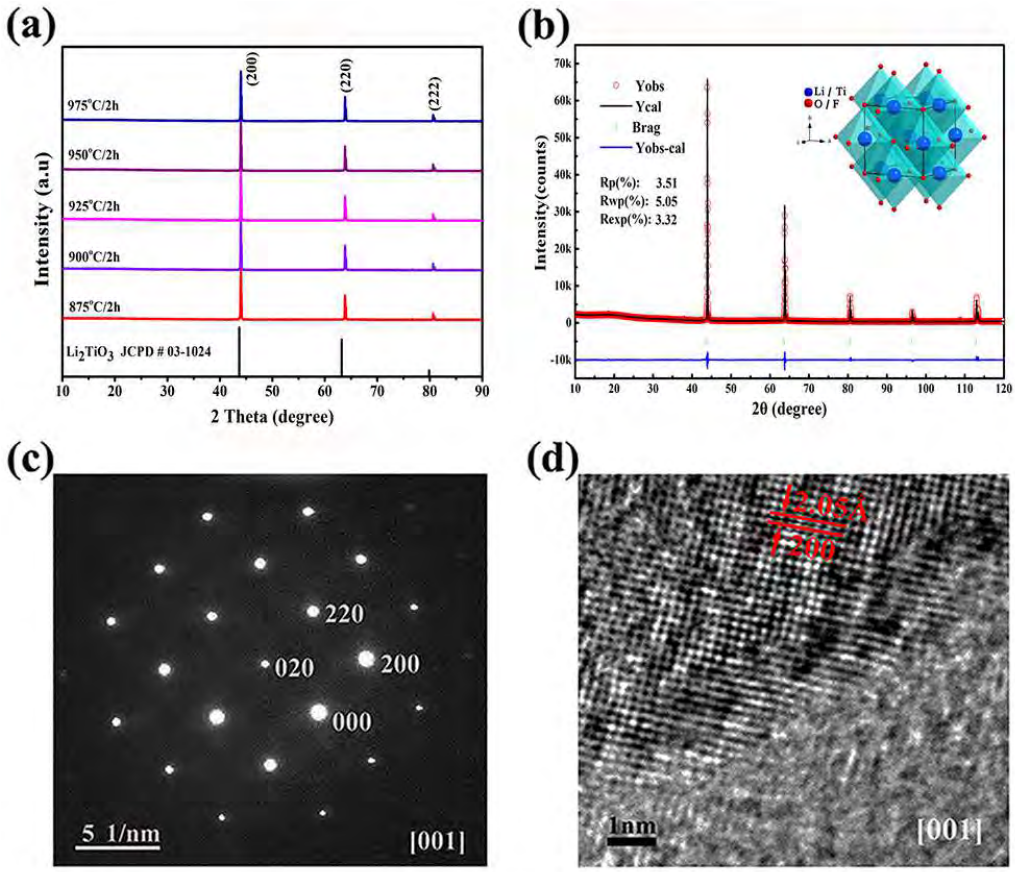

Fig.2

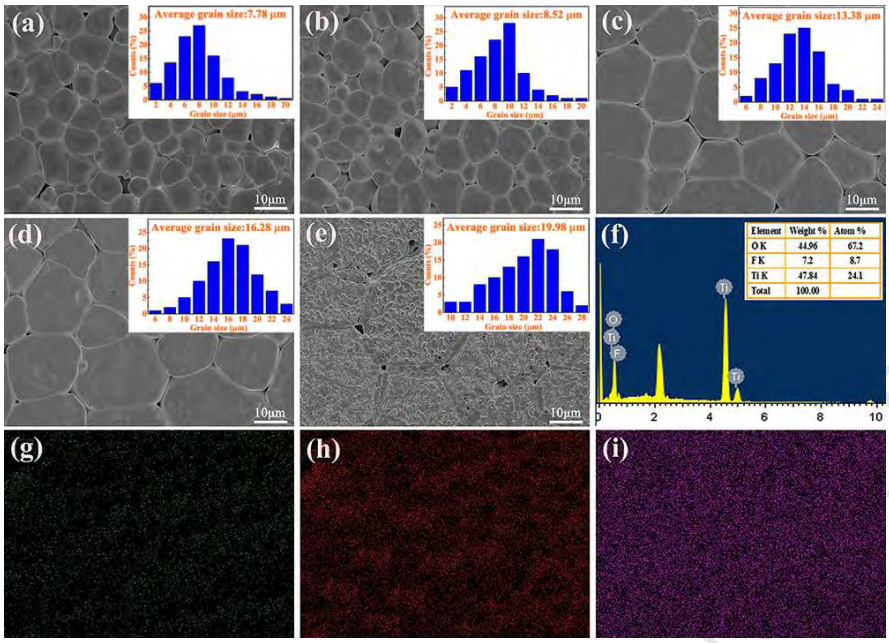

Fig.3

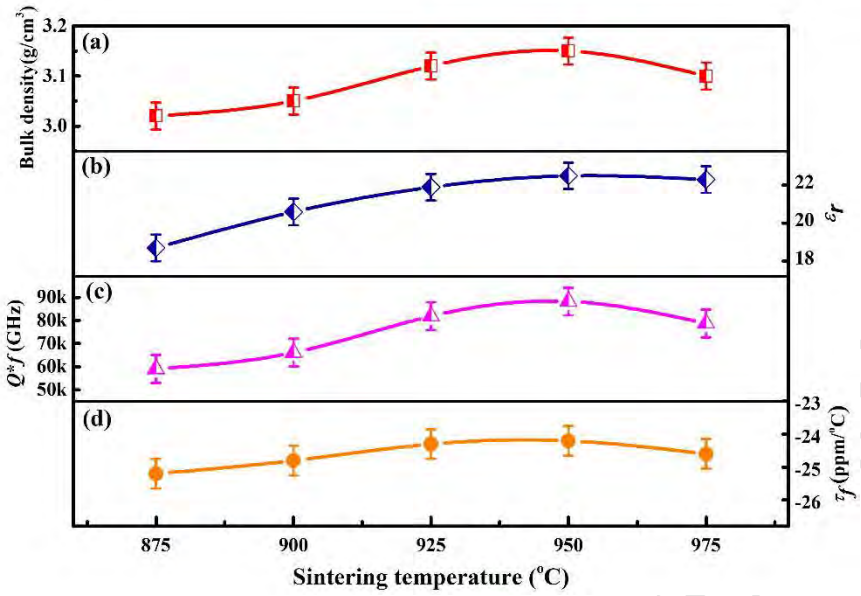

Fig.4

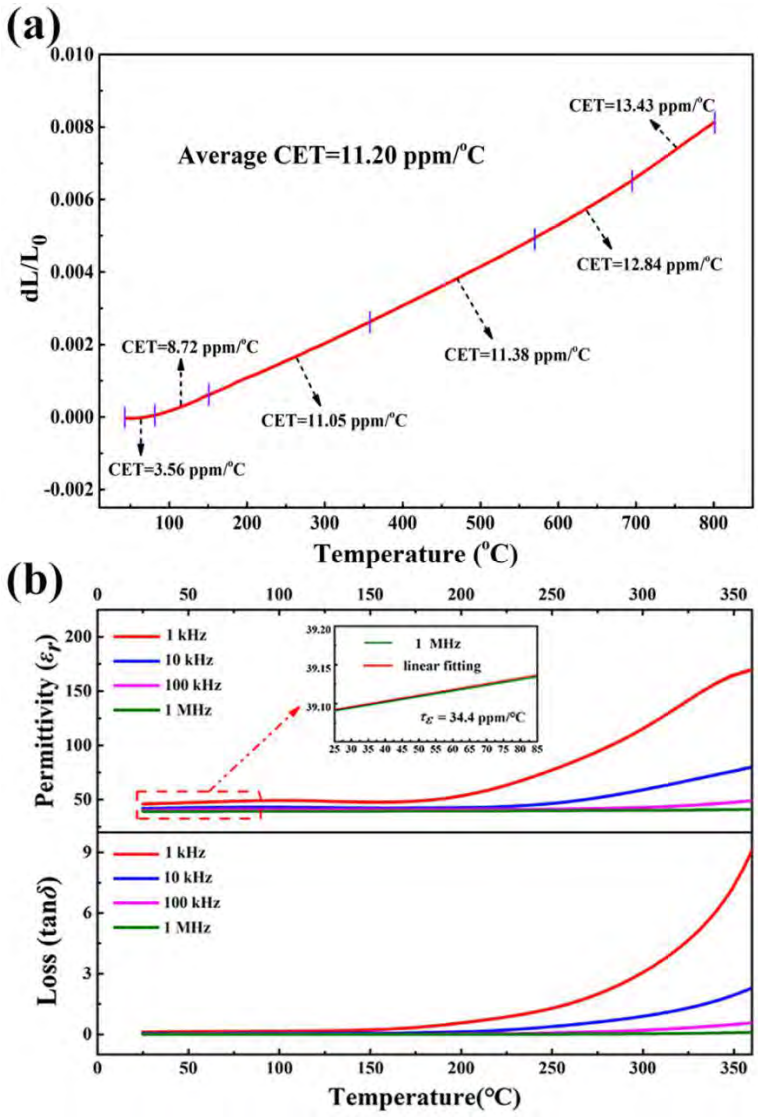
(a)
Average CET=11.20 ppm/°C
CET=13.43 ppm/°C
CET=12.84 ppm/°C
CET=11.38 ppm/°C
CET=11.05 ppm/°C
CET=8.72 ppm/°C
CET=3.56 ppm/°C
dL/L0
Temperature (°C)
(b)
1 kHz
10 kHz
100 kHz
1 MHz
Permittivity (εr)
1 MHz
linear fitting
τε = 34.4 ppm/°C
Loss (tanδ)
Temperature(°C)

Fig.5

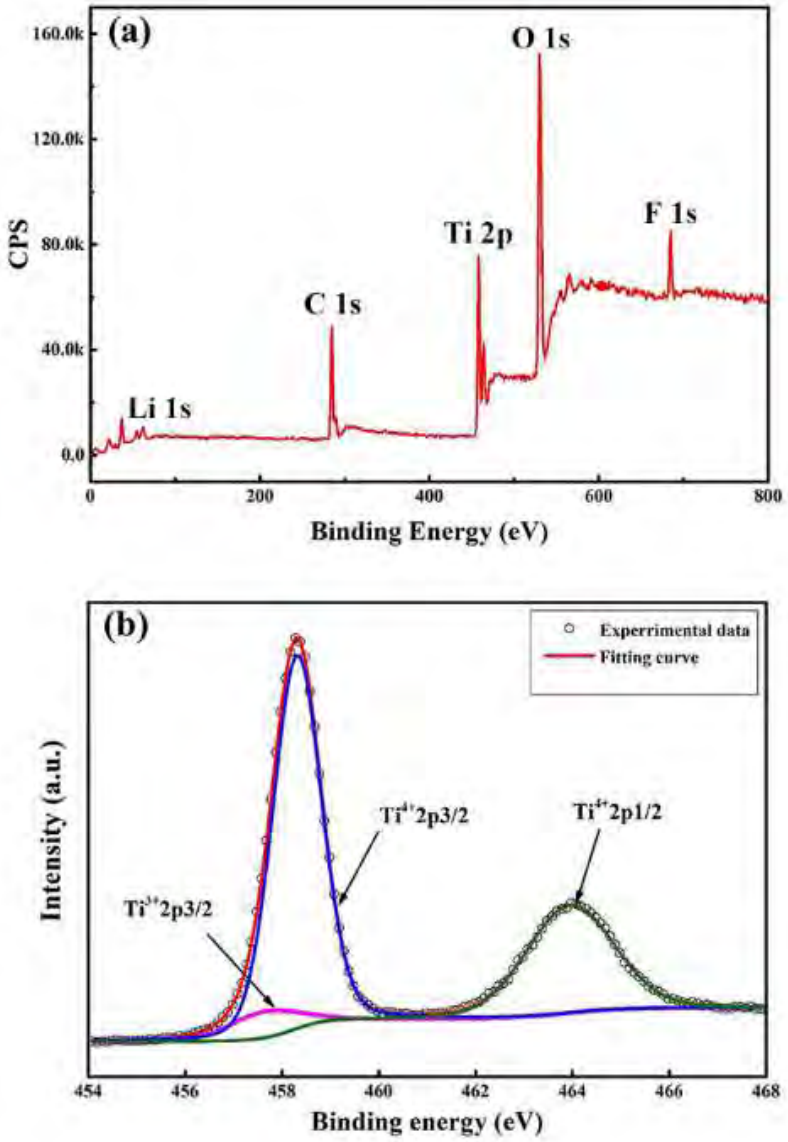
(a)
O 1s
Ti 2p
F 1s
C 1s
Li 1s
CPS
160.0k
120.0k
80.0k
40.0k
0.0
0
200
400
600
800
Binding Energy (eV)
(b)
Experimental data
Fitting curve
Ti4+2p3/2
Ti4+2p1/2
Ti3+2p3/2
Intensity (a.u.)
454
456
458
460
462
464
466
468
Binding energy (eV)

Fig.6

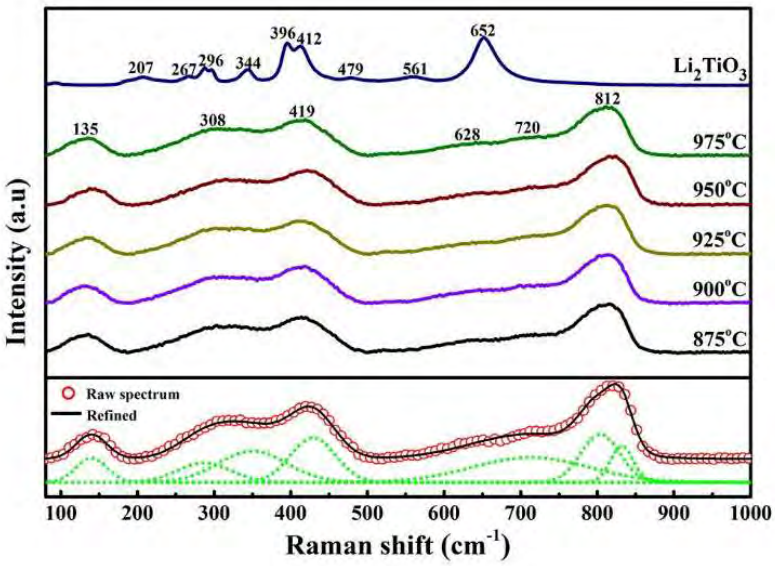

Fig.7

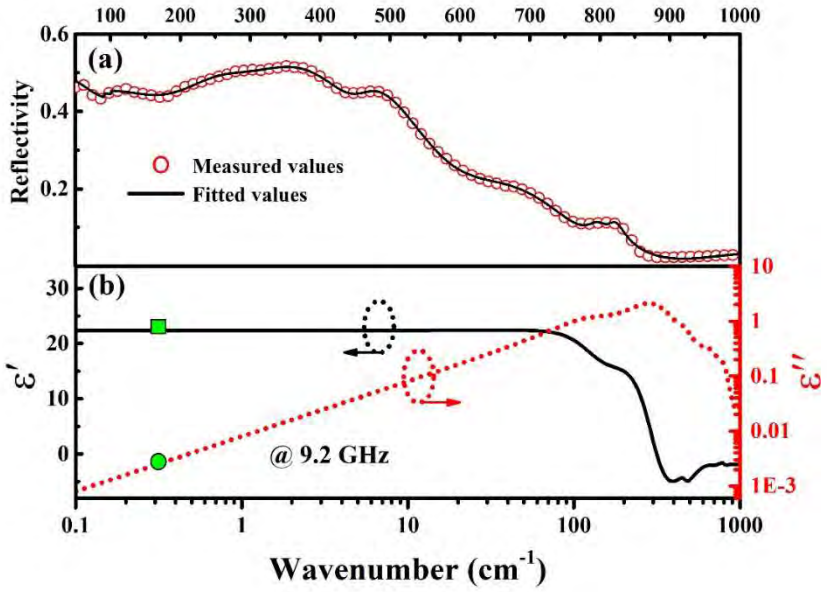

Fig.8